Estimation of Missing Fan-Beam Projections using Frequency Consistency Conditions

Marcel Pohlmann, Martin Berger, Andreas Maier, Joachim Hornegger and Rebecca Fahrig

***Abstract*—Reducing radiation dose is a crucial problem in computed tomography. One approach is to undersample the projections and compensate for the missing ones using an estimation method. In this paper, we introduce a novel method to estimate missing projections in fan-beam geometry. The estimation is done by iteratively enforcing consistency conditions of the sinogram's Fourier-Transform. The completed sinogram can be used for reconstruction using filtered backprojection algorithm to obtain images with less artifact. A comparison of our method to other state-of-the art compensation techniques shows promising results.**

***Index Terms*—Computed Tomography, Sparse Image Reconstruction, Projection Estimation, Spectral Analysis**

I. Introduction

In X-ray computed tomography projections are sampled along a trajectory around the patient. The detector read-out of each view is written row-wise as a set of 1-D projection images, also referred to as sinogram.

In order to reduce the radiation exposure of a patient during a CT scan, the projections can be undersampled by measuring, only a subset of projections. Using filtered backprojection on a undersampled sinogram might produce streak artifacts in the resulting image. To avoid those artifacts a compensation for the missing projections is needed.

Depending on the different imaging geometry every sinogram underlies data consistency conditions, e.g. the well known Ludwig-Helgason consistency condition of the two-dimensional Radon transform. These conditions have already been utilized in the field of image reconstruction from a limited number of view angles [1].

But there are also consistency conditions in the sinogram's Fourier Space, as Edholm et al. showed by their derivation of the frequency-distance relationship for the parallel-beam sinogram [2]. This relationship attributes contributions in sinogram-frequency space to points in the object at fixed distances along the projections. Mazin et al. performed a similar derivation to arrive at corresponding properties of a fan-beam sinogram [3]. In the parallel-beam case as well as the fan- beam case, the derived property is a zero-energy region in the Fourier transform of the full scan sinogram.

In this paper, we present a method that estimates missing projection data of undersampled fan-beam sinograms by utilizing the frequency condition mentioned above.

Rebecca Fahrig is with the Department of Radiology, Stanford University, Stanford, CA, USA. Marcel Pohlmann, Martin Berger, Andreas Maier and Joachim Hornegger are with the Pattern Recognition Lab, Department of Computer Science, Friedrich Alexander Universität Erlangen-Nürnberg. This work has been supported by the Research Training Group 1774 "Heterogeneous Image Systems", funded by the German Research Foundation (DFG).

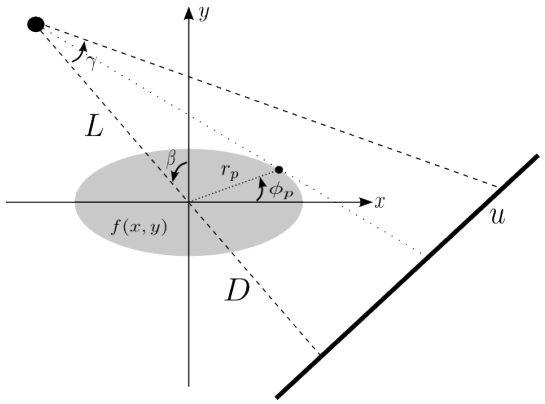

Figure 1. Fan-beam CT geometry with equally-spaced detector used for the estimation of unknown projections

II. Method

A. Background

Our method for the estimation of the missing data is iterative and based on the consistency-conditions of the two-dimensional Fourier transform of the fan-beam sinogram. Iterative methods similar to ours have previously been applied in a variety of other applications where a complete set of data is not available in measurement space but prior knowledge is available in a second space that is related to the first by a simple transformation, in this case the two-dimensional Fourier transformation. This type of iterative algorithm has successfully been implemented in image restoration problems such as band- limited spectral analysis [4], [5] and spectral deconvolution [6], [7]. Another estimation method for SPECT based on the consistency-condition of the two-dimensional Fourier transform of the parallel-beam sinogram is discussed in [8].

B. Theory

Using the geometry shown in Fig. 1 we denote the distance from the origin of a point of interest as r_p and its angle from the x-axis as ϕ_p, the source-to-isocenter distance as L and the isocenter-to-detector distance as D. We can model the object function $f(x, y)$ as a set of many delta function points. Forward projecting each of them we get sinograms each with a single sinusoidal curve. Adding all obtained sinograms of the single points up to one image will give us the observed sinogram. The derivations in [2] and [3] use this decomposition of the sinogram to obtain properties from its Fourier transform. Applying the two-dimensional Fourier

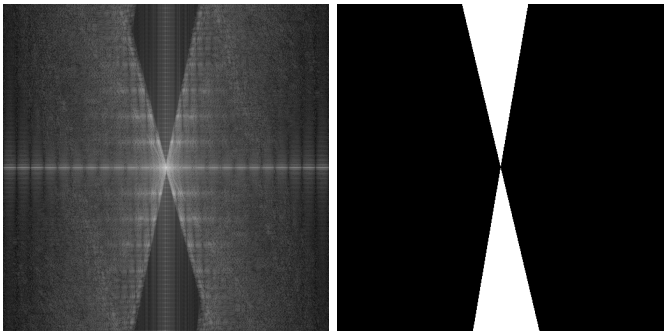

(a) (b)

Figure 2. (a) Appearance of the Fourier transform of a fan-beam sinogram and (b) the corresponding double-wedge filter

transform on a sinogram of an arbitrary delta function will give us

$$P(\zeta,k) \approx e^{-jk(\phi_p+\frac{\pi}{2})} J_k\left((k-(L+D)\zeta)\frac{r_p}{L}\right) \quad , \qquad (1)$$

where J_k denotes a Bessel function of the first kind of order k. Because Bessel functions of order k rapidly tend to zero if the argument is less than k, Eq. (1) implies that the Fourier transform is approximately zero for all frequencies (ζ, k) such that

$$\left|\frac{k}{k-\zeta(L+D)}\right| > \frac{r_p}{L} \quad . \qquad (2)$$

The Bessel function in Eq. (1) is an approximation which was determined intuitively but validated empirically in [3]. Eq. (2) parametrizes a double-wedge region in the frequency domain of the sinogram, containing negligible coefficients. The boundary of this region is described by the equation $\zeta = (k/(L+D))(1 \pm L/r_p)$. The single points of the object within a smaller radius have a larger double-wedge region than single points located at the maximum radius of our object.

Since we are interested in restoring the complete sinogram and not only a region of interest, we interpret r_p as the maximum radius of the object. We can now design a fan-beam double-wedge filter for the estimation of the missing lines in our algorithm. Fig. 2 (a) shows the Fourier transform of a sinogram of an object with $r_p = 200$ mm, the double-wedge region can already be identified and (b) shows the corresponding double-wedge filter.

Modeling the observed sinogram $p(u,\beta)$ as a point-wise multiplication of the non-undersampled sinogram $p_{ideal}(u,\beta)$ with a missing projection mask $w(u,\beta)$, which contains zero-rows if the projection is not measured and ones otherwise, will initially violate the condition of the zero-energy double-wedge region. We can use the designed double-wedge filter to enforce the condition iteratively in the estimation algorithm by cutting of the high frequencies corresponding to the missing projections.

Eq. (1) describes the double wedge region in a continuous manner without respecting discretization problems. For this reason we applied a morphological erosion operation in the direction of ζ on the double-wedge filter. After this pre-processing we can be sure that we will not affect any frequencies that do not correspond to the frequency condition.

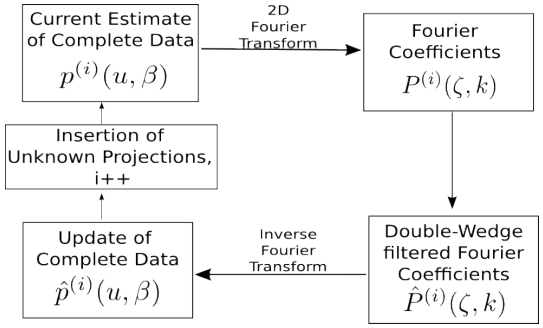

Figure 3. Flow diagram of the iterative double-wedge filtering

C. Algorithm

The main idea of the estimation algorithm is to alternate between the frequency domain to apply the double-wedge filter and the spatial domain to insert the current estimation of the missing projections.

In an initialization step, the observed sinogram has to be extended by the missing projections. Filling the missing rows with the mean value of the observed sinogram turned out to be the best choice. In that way the energy loss caused by the filtering is compensated. It is important to choose the initial values in a way that the Fourier coefficients outside the double-wedge region are not affected, because the algorithm does not perform on these coefficients.

In one iteration step $p^{(i)}(u,\beta)$, the current estimate of the complete sinogram data is zero-padded to the image size of the next power of two and Fourier transformed in order to get the Fourier coefficients $P^{(i)}(\zeta,k)$ with an increased resolution of the frequencies. At this point the eroded double-wedge filter is applied to enforce the condition of zero-energy and eliminate high frequencies referring to the missing projections. The double-wedge filtered Fourier coefficients $\hat{P}^{(i)}(\zeta,k)$ are inverse Fourier transformed to receive a updated version of the complete sinogram $\hat{p}^{(i)}(u,\beta)$ which holds new estimates of the missing projections.

Since the double-wedge filter affects the complete sinogram, we insert only the estimation of the missing projections from $\hat{p}^{(i)}(u,\beta)$ into the sinogram of the next iteration step instead of using the complete data set of the inverse Fourier transform. The iteration procedure, where i represents the current iteration step is repeated until a specific convergence criterion is reached or a fixed number of iterations are performed. The iterative procedure of the algorithm is illustrated in the flow digram shown in Fig. 3.

Source-to-isocenter distance, L	598.5 mm
Detector-to-isocenter distance, D	598.5 mm
# of views over 2π	67, 134
# of detector channels	500
Detector channel spacing	1.0 mm
Maximum radius of object, r_p	200 mm
Kernel width for erosion	7
Resampling factor	2

Table I
SIMULATION PARAMETERS

III. Results

We evaluated the algorithm on simulated data, with a phantom size of 512×512 px, which is shown in Fig. 4 (a). The maximum radius of the overall object extend is $r_p = 200$ mm. In a first experiment, 67 projections, over a full-scan trajectory of 2π, are measured and resampled by the factor of two in order to achieve 134 views for the reconstruction. The results related to this parametrization are shown in Fig. 4. In a second experiment, 134 projections, over the same trajectory, are measured and resampled up to 268 views. The results are shown in Fig. 5. The wedge filter was pre-processed by an morphological erosion operation with a kernel width of 7 px, in the direction of ζ, before applying it on the Fourier coefficients. Additional simulation parameters related to the geometry are listed in Tab. I.

In both experiments, we applied our method on the sparse data with a fixed number of 50 iterations. The result of the iterative double-wedge filter performing on an input number of 67 views is shown in Fig. 4 (c) and performing on an input number of 134 views in Fig. 5 (c). We compared the results to the reconstructions without any compensation and three other estimation techniques: Linear interpolation in the direction of β, Iterative Reconstruction-Reprojection (IRR) [9], where we achieved the best image quality with 3 iterations in the case of 67 projections and 4 iterations in the case of 134 projections, and Spectral Deconvolution [6] with a maximum number of 100 iterations. In all reconstruction results negative values resulting from the FBP have been set to zero, furthermore all pixel values outside of a region of interest corresponding to the detector length have been set to zero as well. We used a Shepp-Logan kernel within the algorithm of IRR and a Ram-Lak kernel for FBP of all final reconstructions. The intensity window for displaying the reconstruction results was chosen to be in the range of 0 to 1 for all images.

In addition to the images of the reconstructions, we calculated the error of the reconstruction with respect to the phantom using normalized root mean square error (NMSRE):

$$NRMSE = \frac{1}{x_{max} - x_{min}} \sqrt{\frac{\sum_{t=0}^{N-1} (x_{1,t} - x_{2,t})^2}{n}} \quad , \quad (3)$$

where x_{min} and x_{max} denote the minimum and maximum intensity value of the phantom. The pixels belonging to the image of the phantom are represented by x_1 and the pixels belonging to the reconstruction are represented by x_2. The NRMSE for the different estimation methods is listed in Tab. II. We implemented the methods using CONRAD [10], a software framework for cone-beam imaging in radiology. To get a picture of the run-time complexity for the methods used in this evaluation, we added the run-time of the estimation methods in Tab. II. Note that the computation of the results for all methods was CPU driven (Intel Xeon X5450, 16 GB RAM).

Compensation Method	**NRMSE**		**Runtime**	
Number of views:	64	134	67	134
Without Compensation	8.02%	4.79%	-	-
Double-Wedge filter	*5.60%*	*3.29%*	*4.68* s	*8.8* s
Linear Interpolation	6.36%	3.61%	-	-
Spectral Deconvolution	6.89%	4.14%	16.55 s	34.12 s
Iterative Reprojection	7.08%	3.69%	234.49 s	467.54 s

Table II
Normalized root mean square error (NRMSE) and run-time of evaluated methods for data completion

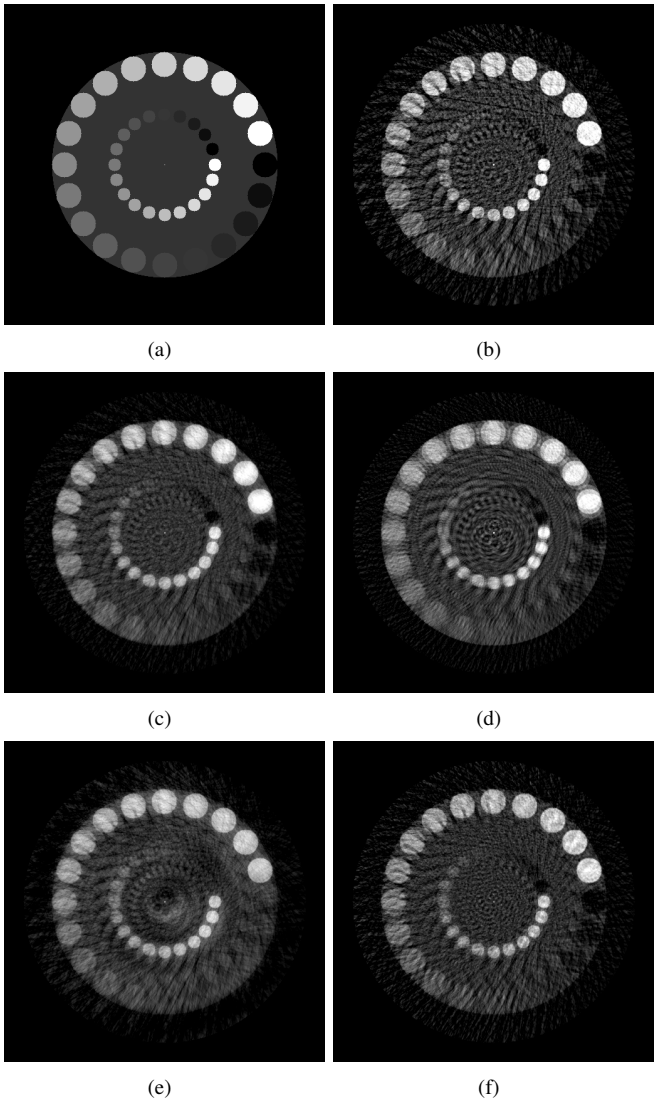

Figure 4. FBP Reconstruction results using different estimation methods for missing projections (a) phantom, (b) reconstruction of the undersampled sinogram with 67 views, (c) reconstruction of the double-wedge filtered sinogram (50 iterations), (d) reconstruction of the linear interpolated sinogram, (e) reconstruction of the sinogram filtered with spectral deconvolution (100 iterations), (f) reconstruction of the completed sinogram using IRR (3 iterations)

IV. Discussion

We presented a new method to estimate missing projections in undersampled sinograms based on the principles of data consistency. In our simulation, the new method performs well

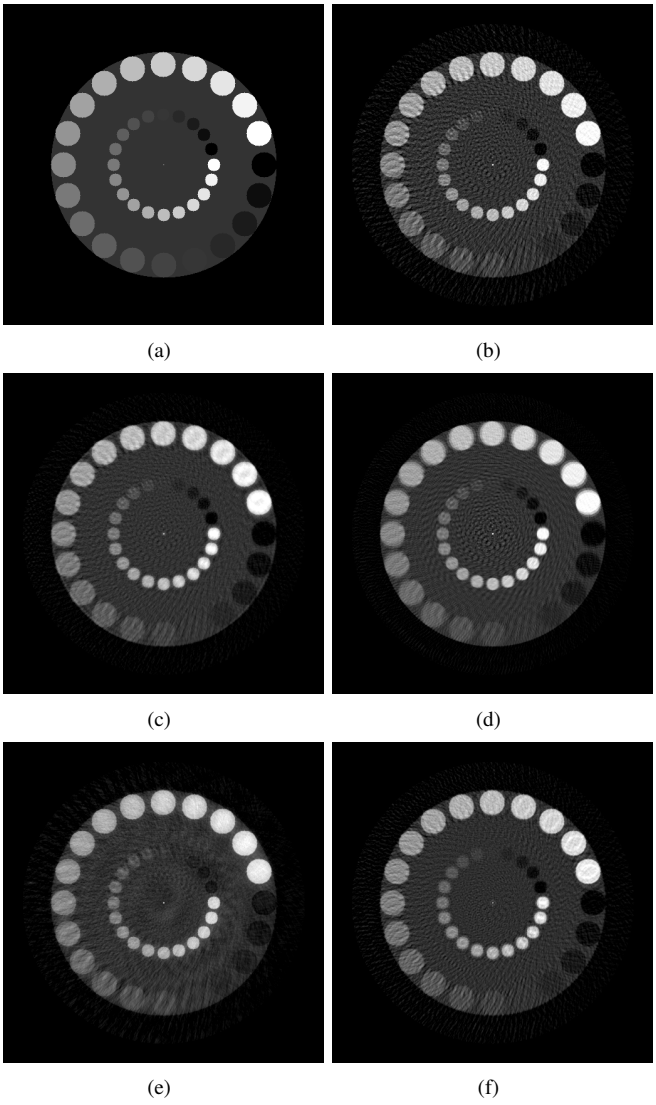

Figure 5. FBP Reconstruction results using different estimation methods for missing projections (a) phantom, (b) reconstruction of the undersampled sinogram with 134 views, (c) reconstruction of the double-wedge filtered sinogram (50 iterations), (d) reconstruction of the linear interpolated sinogram, (e) reconstruction of the sinogram filtered with spectral deconvolution (100 iterations), (f) reconstruction of the completed sinogram using IRR (4 iterations)

even on very sparse projection data. We showed that the estimated projections are consistent with the observed projections and thus result in a reconstruction with a low error. This becomes noticeable in the images of the reconstructions and the values of the NRMSE. In both results of the experiments, it can be seen that the double-wedge filter reduces streak artifacts while preserving the edges of the objects and the their intensity values.

The frequency condition requires a projection set sampled along a full-scan trajectory of 2π in order to satisfy Eq. (1). Usually a projection set from, e.g. a C-arm system, is sampled with 133 projections along a trajectory of 200°. Re-binning this data set to a full-scan data set using data redundancy will provide about 240 projections as input before applying our method. The experiment with an initial number of 134 views, shown in Fig. 5, corresponds to an undersampling of such a C-arm scan and shows promising results. The first experiments with 67 given projections shows that our method also performs good on extremely sparse data sets and its stability does not depend on the input number of projections. Our algorithm is easy to implement and might be embedded as an additional process step in other methods in order to fulfill the data consistency and therefore improve the image quality.

The parameter r_p corresponding to the object extend can directly be measured from the observed sinogram, if the geometry of the scanner is known, using trigonometry.

One limitation of the presented method is that the double-wedge filter estimates parts of the projections in a nearby neighborhood of the periphery of the object more precisely than those referring to the inner part of the object. The inner part can be seen as an object with a smaller extent and therefore requires a larger shape of the double-wedge region. This problem might be solved by iteratively decreasing the parameter r_p that corresponds to a circular region of interest and insert the resulting estimates at the corresponding positions in u-direction into the sinogram. This method will be implemented and evaluated in the future.

In upcoming experiments we are going to investigate the performance of the designed method on real data in order to evaluate the influence of complex structures, noise [11] and scattering [12]. Furthermore, the comparison with regularized iterative methods and additional non-linear filters seems beneficial [13].

The presented method to estimate missing projections in undersampled works well on simulated data. Assuming that the future evaluation using real data shows as promising results as using simulated data, iteratively enforcing consistency condition might be a good approach to reduce the radiation exposure.

REFERENCES

[1] A. K. Louis, "Incomplete data problems in x-ray computerized tomography," vol. 48, no. 3, pp. 251–262, 1986.

[2] P. R. Edholm, R. M. Lewitt, and B. Lindholm, "Novel properties of the fourier decomposition of the sinogram," *Proceedings of the International Workshop on Physics and Engineering of Computerized Multidimensional Imaging and Processing*, vol. Proc. SPIE 671, pp. 8 – 18, 1986.

[3] S. R. Mazin and N. J. Pelc, "Fourier properties of the fan-beam sinogram," *Medical Physics*, vol. 37, no. 4, p. 1674, 2010.

[4] A. Papoulis, "A new algorithm in spectral analysis and band-limited extrapolation," vol. 22, no. 9, pp. 735–742.

[5] A. Papoulis and C. Chamzas, "Detection of hidden periodicities by adaptive extrapolation," *Acoustics, Speech and Signal Processing, IEEE Transactions on*, vol. 27, no. 5, pp. 492–500, 1979.

[6] T. Aach and V. Metzler, "Defect interpolation in digital radiography-how object-oriented transform coding helps," *Medical Imaging*, pp. 17–22, 2001.

[7] H. Kostler, M. Prummer, U. Rude, and J. Hornegger, "Adaptive variational sinogram interpolation of sparsely sampled CT data," in *Pattern Recognition, 2006. ICPR 2006. 18th International Conference on*, vol. 3, 2006, pp. 778–781.

[8] J. S. Karp, G. Muehllehner, and R. M. Lewitt, "Constrained fourier space method for compensation of missing data in emission computed tomography," *Medical Imaging, IEEE Transactions on*, vol. 7, no. 1, pp. 21–25, 1988.

[9] M. Nassi, W. R. Brody, B. P. Medoff, and A. Macovski, "Iterative reconstruction-reprojection: an algorithm for limited data cardiac-computed tomography," *Biomedical Engineering, IEEE Transactions on*, no. 5, pp. 333–341, 1982.

[10] A. Maier, H. G. Hofmann, M. Berger, P. Fischer, C. Schwemmer, H. Wu, K. Müller, J. Hornegger, J.-H. Choi, C. Riess, A. Keil, and R. Fahrig, "CONRAD-A software framework for cone-beam imaging in radiology," *Medical Physics*, vol. 40, no. 11, p. 111914, Nov. 2013.

[11] A. Maier, L. Wigström, H. Hofmann, J. Hornegger, L. Zhu, N. Strobel, and R. Fahrig, "Three-dimensional anisotropic adaptive filtering of projection data for noise reduction in cone beam CT," *Medical Physics*, vol. 38, no. 11, pp. 5896–5909, 2011. [Online]. Available: http://www5.informatik.uni-erlangen.de/Forschung/Publikationen/2011/Maier11-TAA.pdf

[12] B. Bier, A. Maier, H. Hofmann, C. Schwemmer, Y. Xia, T. Struffert, and J. Hornegger, "Truncation Correction for VOI C-arm CT using Scattered Radiation," in *Proceedings of SPIE Medical Imaging 2013: Physics of Medical Imaging*, R. Nishikawa and B. Whiting, Eds., vol. 8668, 2013. [Online]. Available: http://www5.informatik.uni-erlangen.de/Forschung/Publikationen/2013/Bier13-TCF.pdf

[13] C. Riess, M. Berger, H. Wu, M. Manhart, R. Fahrig, and A. Maier, "TV or not TV? That is the Question," in *Fully Three-Dimensional Image Reconstruction in Radiology and Nuclear Medicine*, R. M. Leahy and J. Qi, Eds., 2013, pp. 341–344. [Online]. Available: http://www5.informatik.uni-erlangen.de/Forschung/Publikationen/2013/Riess13-TON.pdf